

Transcriptomic Insights Into Electroacupuncture Using Different Acupoint Combinations to Repair Mucosal Inflammatory Injury Induced in a Rat Model of Gastric Ulcer

Qi Zhang^{1,2}, Tie Li¹, Hailin Jiang¹, Jiazhen Cao³, He Wang¹, Zhongke Wang¹, Qingqing Tang¹, Ning Yang¹, Jinying Zhao¹, Fuchun Wang¹

¹School of Acupuncture and Massage, Changchun University of Chinese Medicine, Changchun City, Jilin Province, People's Republic of China; ²School of Acupuncture and Orthopedics, Hubei University of Chinese Medicine, Wuhan City, Hubei Province, People's Republic of China; ³School of Nursing, Changchun University of Chinese Medicine, Changchun City, Jilin Province, People's Republic of China

Correspondence: Fuchun Wang; Jinying Zhao, School of Acupuncture and Massage, Changchun University of Chinese Medicine, 1035 Boshuo Road, Jinyue District, Changchun City, Jilin Province, 130117, People's Republic of China, Email fuchenwang420@126.com; zhaojinying27@126.com

Background: Electroacupuncture (EA) is a promising treatment for gastrointestinal disorders, yet the efficacy of different acupoint combinations remains mechanistically undefined. We evaluated the therapeutic effects of different acupoint combinations on mucosal inflammatory injury induced in a rat model of gastric ulcer (GU) and dissected its molecular mechanisms through transcriptomic profiling.

Methods: A GU rat model was established using hypothermic restrained water immersion stress. EA therapy was administered to the He-Mu (ST36-CV12), Shu-Mu (BL21-CV12), and Yuan-Luo (ST42- ST40) acupoint combinations for 5 days. EA therapeutic effects were evaluated by coat score, fecal moisture percentage, pain threshold, body mass, organ index, histopathological changes, serum level of oxidative stress, and inflammatory cytokine levels in gastric tissue. A transcriptome analysis identified the related differentially expressed genes (DEGs) and central signaling pathway. Real-time quantitative PCR and Western blot were performed to verify the mRNA and protein expression levels of the main genes in the central pathway.

Results: EA using different acupoint combinations differentially alleviated gastric mucosal injury in GU rats, with the He-Mu group exhibiting superior tissue damage alleviation, as well as inflammation and oxidative stress reductions. A Venn diagram transcriptome analysis revealed a shared central pathway among the three groups, corresponding to focal adhesion. Quantitative validation confirmed that the mRNA, protein, and phosphorylated protein expression of FAK, VCL, and EGFR—the core signal transduction factors of the focal adhesion pathway activated in gastric tissue after EA treatment—were upregulated, consistent with their therapeutic efficacy.

Conclusion: Our results demonstrated that the He-Mu acupoint combination exhibited superior therapeutic efficacy among the three acupoint combinations. EA using different acupoint combinations improved gastric mucosal injury to varying degrees, and was related to the focal adhesion pathway. The *FAK*, *VCL*, and *EGFR* are promising targets, and further studies are needed to elucidate their functional consequences in GU.

Keywords: electroacupuncture, gastric ulcer, acupoint combinations, transcriptome profiling, focal adhesion pathway

Introduction

Gastric ulcer (GU) is a peptic ulcer caused by deep mucosal tissue injury in the gastric mucosa stimulated by gastric acid and pepsin.¹ It is one of the most common gastrointestinal inflammatory diseases, and it has a high incidence and recurrence risk.² According to statistics, the global prevalence of GU is approximately 10%,³ with an annual incidence rate of more than 2.5%.⁴ The incidence of GU among patients with gastrointestinal symptoms is as high as 22.5%.² Within two years after the diagnosis of GU, the risk of gastric cancer increases ten-fold compared with that of the general population,⁵ which imposes a tremendous health and economic burden on society. The pathogenesis of GU is relatively

complex and is generally believed to be closely related to an imbalance between mucosal defense factors and gastric invasion factors.⁶ Long-term ulceration aggravates gastric mucosal injury and causes chronic inflammation, leading to abnormal repair and remodeling of the damaged area, which further stimulates the inflammatory response and promotes disease progression. Therefore, early repair of the damaged gastric may help prevent and treat benign and malignant digestive system diseases.

GU treatment and management has received increasing attention worldwide. The current clinical treatment options are mainly based on pharmacological treatments, including symptomatic treatment with gastric acid inhibitors, gastric mucosal protectants, and antibiotics.⁷ However, the adverse reactions caused by long-term use of these drugs, such as hepatorenal toxicity, gastrointestinal reactions, cardiovascular risks, drug resistance, and drug dependence, limit their use, and there is an urgent need for safer and more effective complementary and alternative therapies.⁸ Acupuncture therapy, a non-drug traditional Chinese medicine technique, has been applied in clinical practice in more than 160 countries and has become a mainstream complementary and alternative therapy worldwide.⁹ Acupuncture therapy is widely used to treat various gastrointestinal diseases to improve gastrointestinal function, and is known for its efficacy and safety.^{10,11} Acupuncture is a complex intervention method that involves specific techniques. Clinical studies have demonstrated that electroacupuncture (EA) is superior to manual acupuncture for improving the outcome of ulcerative diseases.¹² EA combines traditional acupoint stimulation with modern electrical stimulation, which both stimulates acupoints and regulates neuroelectrophysiology. It is a potential treatment for inflammatory pain and has received increasing attention in clinical practice.^{13–16}

The selection of acupoints affects the efficacy of acupuncture. Acupoint combinations are a key aspect of the theory and clinical efficacy of acupuncture. Studies on the effects and mechanisms of different combinations have always been a focus of acupuncture.¹⁷ GU is a disease affecting the meridian, visceral, and abdominal systems. Because of these three types of symptoms, three pairs of classic acupoint combinations were used in this study: “Yuan-Luo acupoint combination treatment of meridian pain disease”,¹⁸ “Hu-Mu acupoint combination treatment of visceral disease”,^{19,20} and “Shu-Mu acupoint combination treatment of lumbo-abdominal disease”.²¹ There are differences in the clinical therapeutic efficacy of these acupoint combinations, but the mechanism underlying these difference is unclear. To determine these mechanisms, we must consider both the macro basis of traditional Chinese medicine, and the micro focus of modern research.

Transcriptome sequencing technology is a research method used to reveal the common and distinct regulatory mechanisms of molecular interactions by measuring gene expression levels and identifying DEGs and related signaling pathways.²² This study was performed to further increase the clinical efficacy of acupuncture treatment for GU. Specifically, the optimal acupoint combination was determined by analyzing the extent to which EA with different acupoint combinations alleviated mucosal inflammatory injury in a rat model of GU. The mechanism of this difference was analyzed based on the differential expression of genes under the action of different factors. This study aimed to provide data support and decision-making references for modern clinical treatment of GU.

Materials and Methods

Main Reagents and Instruments

Primary antibodies against FAK (BS-20735R) and *p*-FAK (BS-3159R) were purchased from BIOSS (Beijing, China), and antibodies against VCL (GB111328), EGFR (GB11084), p-EGFR (GB13213-1), and GAPDH (GB15004) were purchased from Servicebio (Wuhan, China). ELISA kits of IL-4 (MM-0191R1), IL-6 (MM-0190R1), IL-10 (MM-0195R1), IFN- γ (MM-0198R1) were provided by MEIMIAN (Jiangsu, China). Biochemical kits of SOD (A001-1), NO (A013-2), and MDA (A003-1) were provided by Nanjing Jiancheng Bioengineering Institute (Nanjing, China). Hematoxylin-eosin (HE; G1076) and alcian blue-periodate Schiff (AB-PAS; G1049) staining kits were purchased from Servicebio (Wuhan, China). The main instruments included a Novaseq 6000 sequencer (Illumina, USA), an Enspire multimode microplate reader (PerkinElmer, USA), an ST16R high-speed refrigerated centrifuge (Thermo Fisher Scientific, USA), an SPX70BIII biochemical incubator (Fesford Instruments, Hebei, China), Hwato aseptic acupuncture needles, and a Hwato SDZ-II electroacupuncture instrument (Suzhou Medical Instruments, Suzhou, China).

Animal Ethics and Study

All procedures were approved by the Animal Ethics Committee of Changchun University of Chinese Medicine (approval #2022422) and were conducted in accordance with the *NIH Guide for the Care and Use of Laboratory Animals*. Specific pathogen-free healthy male Wistar rats aged 10–12 weeks, weighing 220–240 g, were purchased from Changsheng Biotechnology Co., Ltd. (SCXK (Liao) 2020–0001, Liaoning, China). The rats were housed in the Animal Experimental Center of Changchun University of Chinese Medicine (SYXK (Ji) 2018–0014, Jilin, China) and had access to a standard diet and water ad libitum. The housing environment was maintained at a constant temperature of 25°C±3°C and relative humidity of 55%±5%, with a standard 12-hour light/dark cycle. Before commencing the experiment, rats were acclimated to the conditions of the experimental facility for 5 days. The rats were then randomly divided into five groups (n=7 per group, n=35 total): normal control group (control), GU group (model), GU+He-Mu acupoint combination group (H-M), GU+Shu-Mu acupoint combination group (S-M), and GU+Yuan-Luo acupoint combination group (Y-L).

Generation of the GU Rat Model

The hypothermic restrained water immersion stress (HRWIS) method was used to prepare the GU rat model.^{23,24} The rats underwent 24 hours of fasting, with access to water provided. After anesthesia with 3% isoflurane was administered via inhalation, the rats were quickly fixed in a vertical rat fixator, with their heads facing upward. They were then placed vertically in cold water at 4°C, ensuring that the water level was even with the rat's xiphoid process. The rats were then placed in a 4°C constant temperature refrigerator for 4 hours.

EA Treatment

GU has a certain ability for self-healing, with recovery typically taking more than 7 days.^{25,26} The analgesic effect of acupuncture is affected by the duration of the needle retention. During the 30-minute acupuncture cycle, the analgesic effect of acupuncture initially increased, then decreased, followed by another increasing before finally declining. The greatest change in pain threshold occurred when the needles were retained for 15–20 minutes, indicating that the analgesic effect reached the maximum effect.^{27,28} Based on these results, EA treatment was started the day after modeling and continued daily for 5 days, with each session lasting 20 minutes. Prior to EA, the rats were anesthetized with 2% isoflurane for maintenance. The H-M group was treated with a combination of ST36 (Zusanli, located 3 mm below and lateral to the fibular head on the posterolateral knee joint of the posterior lower extremity) and CV12 (Zhongwan, 20 mm above the umbilicus). The S-M group was treated with a combination of BL21 (Weishu, on the lower sides of the 12th thoracic vertebra, 6 mm lateral to the dorsal median line) and CV12. The Y-L group was treated with a combination of ST42 (Chongyang, the highest point between the second and third metatarsals in the instep) and ST40 (Fenglong, lateral to the posteroinferior aspect of the leg, at the midpoint of the line between the lateral malleolus and the lateral depression of the patellar ligament). Conventional acupoint selection methods, according to location, included near and far acupoints, local acupoints, and distal acupoints. Previous studies showed that the He-Mu, Shu-Mu, and Yuan-Luo acupoint combinations, which were representative of traditional acupoint methods and commonly used classic acupoint pairs in clinical practice, had significant effects in treating gastrointestinal diseases.^{10,29} Additionally, both clinical^{30,31} and animal studies^{32,33} confirmed the effectiveness of these combinations in treating GU. Previous studies also showed that there was a linear relationship between the intensity of electrical stimulation and the distance of treatment, with the minimum safe distance determined at the lowest current electrical stimulation intensity of 1 mA.³⁴ Frequencies between 1 and 100 Hz can stimulate a nerve tissue response. In clinical practice, a 2/100 Hz sparse-dense wave is often selected to maximize an analgesic effect.^{35,36} Based on these characteristics, along with the rats' tolerance and the demand for a sustained analgesic effect, the following EA parameters were selected for this study: sparse-dense wave, 2/20 Hz vibration frequency, and 1 mA intensity. To avoid current passing through the heart, an auxiliary acupuncture needle was placed 2–3 mm proximal to the CV12 in the H-M and S-M groups. Acupuncture needles were inserted into both sides of the acupoints to a depth of 1–3 mm. Subsequently, the needle handles were connected to the EA device, with the two acupoints on the same side connected to the positive and negative poles of the EA instrument—upper and lower poles—respectively. The sparse-dense wave was then applied. All groups were maintained under consistent anesthesia and fixation during this intervention. After the treatment concluded (day 12), the rats were sacrificed using a 5% isoflurane overdose, and tissue samples were collected.

Behavioral Assessment

After the intervention, the coat score, fecal moisture percentage, and pain threshold (using a hot plate) of the rats in each group were obtained.

Coat Score Test

The rat coat score of the rats was obtained by dividing the coat into six sections (head, neck, trunk back, abdomen, forelimb, and hindlimb) and scoring each section. The filth, molt, and knots in each section were observed. The scores were recorded from 0–1 point per section, with a high score of 6 points.

Fecal Moisture Percentage Test

The rat feces were collected and weighed to obtain the wet weight of the feces. After drying in an oven at 60°C for 4 h, the dry weight of the feces was obtained. The fecal moisture percentage was calculated as follows:

$$\text{Fecal Moisture Percentage} = \frac{(\text{wet weight of feces} - \text{dry weight of feces})}{\text{wet weight of feces}} \times 100\%$$

Hot Plate Pain Threshold Test

Rats were placed on a smooth test bench, with their tails flat on the test bed of the photothermal tail pain instrument. The distal one-third of the tail was positioned at the luminescent point of the instrument. The thermal stimulation light source was activated, and the photothermal stimulation was stopped when the rats showed strong tail flick behavior. Each test was separated by a 10 minute interval, and the average of three tests was used as the result. The photothermal intensity was maintained at a constant level, with a power of 30% and an upper time limit of 10s.

Body Weight and Organ Indices

The body weight of each rat was measured before and after modeling, as well as during the treatment period. The stomach, liver, spleen, and thymus tissues were rinsed with saline solution (0.9% sodium chloride) and then weighed. The organ indices were calculated according to the organ and body weights of the rats.

Macroscopic Assessment of Gastric Ulcers

The degree of gastric mucosal injury was determined based on a published procedure.³⁷ Briefly, the gastric tissue was incised along the greater curvature, and the mucosa was turned inside out and perform macroscopic observations of gastric mucosal damage. Gastric tissue photographs were analyzed using Image J software. The Guth grading criteria were applied to obtain macro scores, which were obtained to determine the ulcer index (UI) and the ulcer inhibition ratio (UIR) of the animals.

The UI was calculated as follows:

$$\text{UI} = \text{spot erosion score} + \text{erosion length score} + \text{erosion width score}$$

The UIR rate was calculated as follows:

$$\text{UIR} = \frac{(\text{model UI} - \text{treatment UI})}{\text{model UI}} \times 100\%$$

Histopathological Analysis of Gastric Tissue

Gastric tissue was submerged in a 4% paraformaldehyde solution for 24 hours, then removed for ethanol gradient dehydration, xylene treatment for transparency, paraffin embedding, and sectioning. Following this, HE and AB-PAS staining were performed. The histopathological morphology of the gastric mucosa and the secretion of mucus substances in each group of rats were observed under a microscope.

Level of Inflammatory Factors and Oxidative Stress

ELISA kits were used to determine the gastric tissue levels of inflammatory mediators, including IL-4, IL-6, IL-10, and INF- γ . Biochemical kits were used to measure the levels of SOD, NO, and MDA in serum as surrogate markers of oxidative stress. The specific procedures strictly adhered to the manufacturer's instructions.

RNA-Seq Data Analysis

RNA Extraction From Gastric Tissue and Preparation for Sequencing

Gastric tissue ($n = 5$ per group) was excised,³⁸ and total RNA was isolated using Trizol reagent according to the manufacturer's instructions. The concentration, purity, and integrity of the total RNA were evaluated by spectrophotometry, fluorescence analysis, and agarose electrophoresis, respectively. After passing the quality control check, 3 μg of total RNA was used to construct the transcriptome sequencing library. The final cDNA library was constructed by mRNA enrichment, purification, fragmentation of mRNA, synthesis of the first and second strands of cDNA, end-repair, and fragment enrichment by polymerase chain reaction (PCR) amplification.

Processing of Sequencing Data

Next-generation sequencing using paired-end sequencing was performed on an Illumina sequencing platform to generate raw data. The raw data were subsequently saved and filtered to obtain clean data. The quality of the sequencing data was assessed using FastQC. HISAT2 software was used to align clean reads to the reference genome and determine gene expression levels based on fragments per kilobase of transcripts per million mapped read (FPKM) values.

DEGs and Their Functional Enrichment Analysis

DESeq2 software was used to analyze the differences in gene expression, and the DEGs were screened using $|\log_2 \text{fold change}| > 1$, and $p < 0.05$ to define the significance threshold. Gene Ontology (GO) annotation and Kyoto Encyclopedia of Genes and Genomes (KEGG) pathway enrichment analysis were used to identify DEGs from the previous step, with $p < 0.05$ as the significant enrichment criterion. Venn diagram analysis was performed to identify the core pathway of the co-interactions.

Determination of Gene Expression Using Real-Time Quantitative Polymerase Chain Reaction (RT-qPCR)

The mRNA expression of key genes (*FAK*, *VCL*, and *EGFR*) in the DEGs core pathways were examined by RT-qPCR. Total RNA was extracted from the gastric tissue of each group using TRIZOL reagent. cDNA was synthesized using a HiScript[®] II Q RT SuperMix for qPCR (+gDNA wiper) reverse transcription kit. RT-qPCR reactions were performed with SYBR Green master mix on an ABI Step One system. The reaction conditions were as follows: an initial denaturation step at 95°C for 10 minutes, followed by 40 cycles of denaturation at 95°C for 15 seconds, annealing at 60°C for 60 seconds, and elongation at 72°C for 30 seconds. *GAPDH* was used as the internal control, and the relative expression of the target gene was calculated using the $2^{-\Delta\Delta C_t}$ method. The primer sequences (5'-3') were as follows: *FAK* forward: GCTTAATCTGGCCAGGACGG, reverse: TGAAGCACGGTTTGAGAGGT; *VCL* forward: GGTGCTGCCAATAAATCG, reverse: CCTTACACTTGTCCAGGTCTT; *EGFR* forward: TACGCCTTAGCCGTCCTGTC, reverse: GTTCTCCTCTCCTCTTCCCC; and *GAPDH* forward: ACAGCAACAGGGTGGTGGAC, reverse: TTTGAGGGTGCAGCGAACTT.

Protein Expression Determination Using Western Blot (WB)

Protein expression levels (*FAK*, p-*FAK*, *VCL*, *EGFR*, and p-*EGFR*) of key genes in the DEGs core pathways were determined by WB. Gastric tissue was lysed using RIPA lysis buffer and homogenized at 4°C. The supernatant was collected, and a bicinchoninic acid assay was performed to determine the protein concentration. Subsequently, polyacrylamide gel electrophoresis was performed, followed by membrane transfer and blocking with 5% skim milk. The membrane was incubated overnight at 4°C with antibodies against *FAK*, p-*FAK*, *VCL*, *EGFR*, p-*EGFR*, and the internal reference *GAPDH* individually. After washing with Tris buffered saline with Tween, a horseradish peroxidase-labeled

secondary antibody was added, and the membrane was incubated on a shaker at room temperature for 2 hours, followed by ECL luminescence color development. The optical density of the target band was analyzed using a gel image analyzer.

Statistical Analysis

Data are presented as mean \pm standard deviation (SD). Statistical analysis and graph creation were performed using GraphPad Prism 9.0 (San Diego, CA, US). Normality and variance chi-square tests were initially performed on all data. ANOVA was carried out between groups using one-way ANOVA, and post-hoc multiple comparisons were performed using the LSD test, with $p < 0.05$ considered statistically significant.

Results

Effects of Different Acupoint Combinations of EA on Rats With GU

Daily Behavioral Observations and Organ Indices

The GU rat model was established, and daily observations of the rats' appearance and behavior in the different acupoint combination groups during EA treatment were recorded. A schematic diagram of the experimental timeline is illustrated in [Figure 1A](#). The rats in the control group exhibited good mental condition, were active and agile, and had glossy coats, maintaining a healthy diet and normal excretion. As shown in [Figure 1B–E](#), after modeling, the rats in the model group exhibited low energy levels, weight loss, accompanied by noticeable signs of gastrointestinal dysfunction, including messy fur, thin and soft stools, and behaviors reflecting internal organ pain. These symptoms confirmed the successful establishment of the GU model induced by low-temperature restrained water immersion stress method. In contrast, rats in the acupoint combination groups showed varying degrees of improvement in mental condition, body weight, and gastrointestinal function compared to the model group. In particular, the gastrointestinal dysfunction characteristics of rats in the H-M group were significantly reduced compared with those of the model group. Visceral pain caused by gastric mucosal injury generates an inflammatory response, leading to swelling of target organ tissue and abnormal immune function, and thus increasing the organ indices.³⁹ In the present study, the liver, spleen, thymus, and stomach organ indices were lowest in the control group and highest in the model group ($p < 0.001$) ([Figure 1F and G](#)), indicating that gastric mucosal injury caused by GU resulted in congestion and swelling of gastric tissue and immune organs in rats. Notably, the increased organ indices in the model group indicated the presence of inflammatory pathological changes, such as congestion and edema of the tissue structure. The decreased organ indices in the different acupoint combination groups suggested that EA improved the inflammation and edema in the gastric and immune organs of GU rats, and that it had exerted a certain immunomodulatory effect on systemic oxidative damage and inflammatory response.

Gastric Histopathological Changes

In this study, histopathological observations of gastric tissue were performed to assess the degree of damage to the tissue. The effects of EA on the morphology of the gastric tissue in rats in the different acupoint combination groups are shown in [Figure 2A](#). The UI was evaluated by observing the morphological changes in the gastric tissue, and the UIR was calculated ([Figure 2B](#)) to analyze intragastric ulceration in rats from a macroscopic perspective. The surface of the gastric tissue in the control group was not damaged, had a clear structure with a ruddy color, and remained in a healthy state. Gastric tissue from rats in the model group exhibited multiple large linear and lamellar ulcerated surfaces, accompanied by mucosal edema. After treatment with EA, the congestion and swelling of the gastric mucosa and the area of ulceration were reduced to varying degrees, with the lowest degree of damage in the H-M group, in which ulcers were sporadically distributed. As shown in [Figure 2B](#), compared to the control group, the UI was significantly increased in the model group, but was significantly reduced by EA in the different acupoint combination groups compared with the model group, particularly the H-M group ($p < 0.001$). The average UIR of the H-M, S-M, and Y-L groups were 78.60%, 56.03%, and 21.52%, respectively.

We performed a gastric histological analysis using two different stains ([Figure 2C and D](#)) to reveal the microstructure and functional changes in the intragastric ulcerated tissue and cells at the microscopic level. The pathological changes in the gastric mucosa were observed by HE staining, while the synthesis and secretion of mucin in gastric mucosal epithelial cells were detected by AB-PAS staining to determine the degree of damage to the gastrointestinal mucus layer. HE staining ([Figure 2C](#)) showed that the structure of the gastric mucosa in the

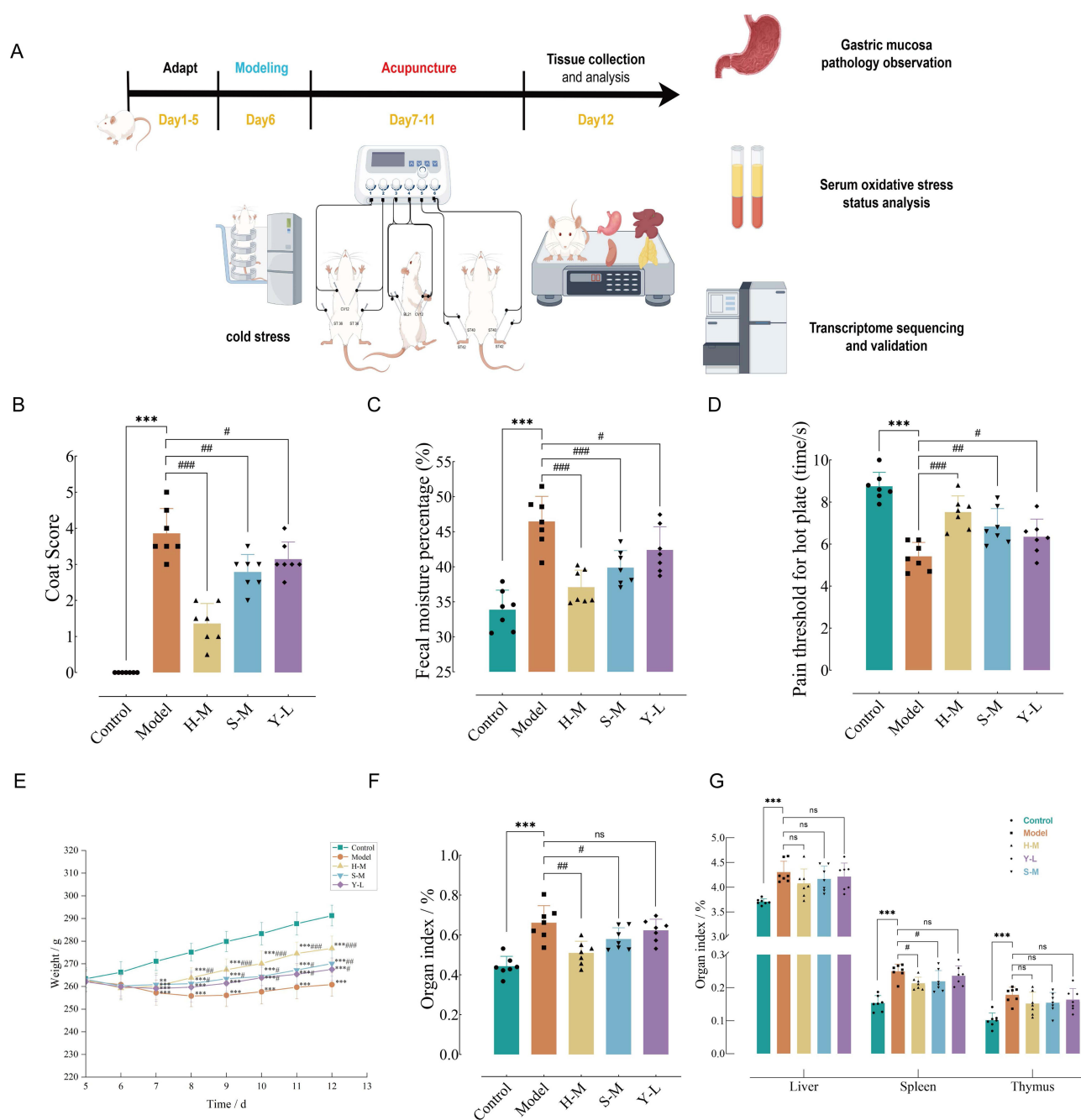


Figure 1 Effects of duration and EA using different acupoint combinations on body weight and organ indices. **(A)** Schematic showing the establishment of the GU rat model and the EA treatment schedule. **(B)** Coat score test (n=7 per group). **(C)** Fecal moisture percentage test (n=7 per group). **(D)** Hot plate pain threshold test (n=7 per group). **(E)** Trends in body weight change (n=7 per group). **(F)** Gastric organ indices (n=7 per group). **(G)** Immune organ indices (liver, spleen, and thymus) (n=7 per group). *** $p < 0.01$ and ** $p < 0.001$ vs control group; # $p < 0.05$, ## $p < 0.01$, and ### $p < 0.001$ vs model group.

control group was intact, flat, and smooth, with the glands evenly arranged. In the model group, severe congestion, edema, and inflammatory cell infiltration were observed in the submucosa of the gastric tissue. Rats in the EA groups with different acupoint combinations showed fewer signs of capillary dilatation, congestion, and inflammation, with partially repaired mucosa. AB-PAS staining (Figure 2D) showed that neutral mucins present in the gastric mucosa of the control group stained red, whereas in the model group, large amounts of blue-stained acidic mucin and violet-stained mixed mucin were observed. Compared with the model group, the area and depth of blue and violet staining decreased visibly in the different acupoint combination groups, and the H-M group showed significant regression. These results demonstrated that EA with different acupoint combinations effectively

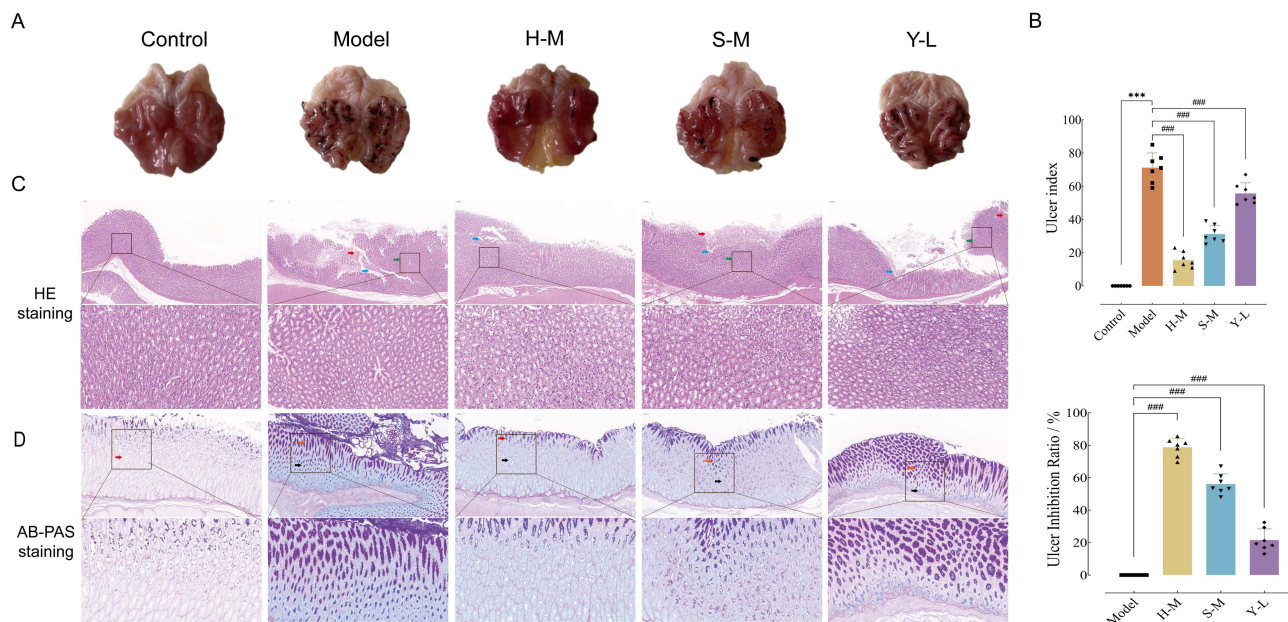


Figure 2 Effects of EA using different acupoint combinations on macromorphology and micromorphology of rats with GU. **(A)** Macroscopic morphology of the gastric mucosa in rats from different groups. **(B)** UI and UIR in rats from each group ($n=7$ per group). **(C)** HE staining of gastric tissues from rats in different groups (Above: scale bar = 100 μm , magnification $\times 100$; below: scale bar = 20 μm , magnification $\times 400$). Blue arrows indicate loosely arranged connective tissue, red arrows indicate capillary hyperplasia and hemorrhage, and green arrows indicate marked edema. **(D)** AB-PAS staining of gastric tissues from rats in different groups (Above: scale bar = 50 μm , magnification $\times 200$; below: scale bar = 20 μm , magnification $\times 400$). Red arrows indicate neutral mucin, black arrows indicate acidic mucin, and yellow arrows indicate mixed mucin. $***p < 0.001$ vs control group; $####p < 0.001$ vs model group.

improved the general state and macroscopic characteristics of gastric tissue in GU rats and reversed the pathological state of the gastric mucosa, with the most significant therapeutic effect observed with the H-M acupoint combination.

Inflammatory Cytokines and Oxidative Stress

Because an inflammatory reaction and increased oxidative stress were key drivers of GU pathophysiology,⁴⁰ changes in these factors were measured after EA treatment using different acupoint combinations. Regulating the imbalance of pro-inflammatory and anti-inflammatory cytokines in the body is an important means of preventing and treating GU.⁴¹ Gastric mucosal injury induced a notable increase in the concentrations of gastric pro-inflammatory cytokines ($p < 0.001$), including IL-6 and INF- γ , and significantly reduced the gastric concentrations of anti-inflammatory cytokines ($p < 0.001$), including IL-4 and IL-10. However, compared with the model group, the levels of IL-6 and INF- γ significantly decreased ($p < 0.001$), and the levels of IL-4 and IL-10 significantly increased ($p < 0.01$) in the different EA acupoint combination groups, with the H-M group demonstrating the best results ($p < 0.001$) (Figure 3A).

The levels of the antioxidant enzyme SOD, oxygen free radical NO, and lipid peroxidation-product MDA are important indicators of oxidative stress injury in the body.⁴² As shown in Figure 3B, gastric mucosal injury induced in the model group decreased SOD activity and the NO level ($p < 0.001$), and increased the MDA level in serum compared with the control group ($p < 0.001$). Compared with the model group, the changes in these levels in the different acupoint combination groups were attenuated, with the most significant result in the H-M group ($p < 0.05$).

Collectively, EA intervention with all three acupoint combinations was able to repair the gastric mucosal damage and improve the anti-inflammatory and antioxidant capacity in GU rats, with the H-M group showing the greatest protective effect.

Transcriptome Profiling Revealed Gene Expression Changes Quality Control of RNA Samples and Sequencing Data

We performed transcriptome profiling on 25 gastric tissue samples ($n=5$ per group) to characterize the gene expression changes regulated by EA in the different acupoint combination groups. Sequencing of the samples yielded high-quality

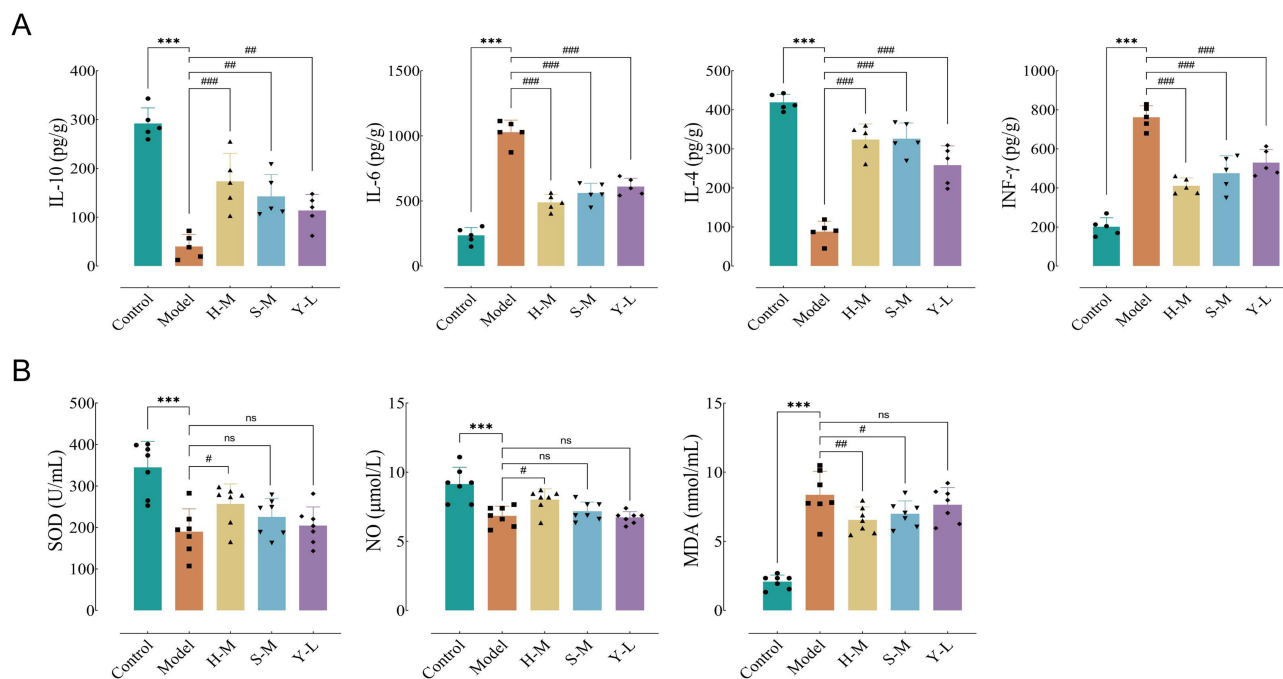


Figure 3 Effects of EA using different acupoint combinations on inflammatory cytokines and oxidative stress markers. **(A)** Effects of EA using different acupoint combinations on inflammatory cytokines (IL-10, IL-6, IL-4, and INF- γ) in gastric tissue, measured by ELISA assays ($n=5$ per group). **(B)** Effects of EA using different acupoint combinations on oxidative stress markers (SOD, NO, and MDA) in serum ($n=7$ per group). *** $p < 0.001$ vs control group; # $p < 0.05$, ## $p < 0.01$, and ### $p < 0.001$ vs model group.

clean reads. As detailed in Supplementary Table S1 and [Figure S1](#), we obtained a total of 175.77 GB of clean data, with each sample containing as much as 7.03 GB of high-quality data. The clean ratio of all samples was $> 98.19\%$. Additionally, the proportion of bases with a sequencing error rate below 1% (Q20) was $> 97.92\%$, while the proportion with a sequencing error rate below 0.1% (Q30) was $> 95.61\%$, and the GC content was approximately 48.45%–51.78%. These results indicated that the sequencing data and assembly quality met the stringent criteria established for this study, thus ensuring the reliability and accuracy of the findings.

Transcriptome Analysis Identified Significant DEGs

The correlation coefficients from a Pearson correlation analysis ranged from 0.4192 to 1.000, with principal component classifications > 0.8 among all the biological replicates ([Figure 4A](#)). Principal component analysis (PCA) showed that the first and second principal components accounted for 54.2% and 33.4% of the variance, respectively, and that sample clustering was distinct ([Figure 4B](#)). These results indicated that the groups of samples were highly reproducible and that the RNA-seq data met the stringent criteria required for this study, thus ensuring reliability and accuracy of the findings.

DEGs were using the expression difference multiplicity $|\log_2 \text{fold change}| > 1$ and corrected significance of $p < 0.05$, resulting in a total of 23,096 DEGs. The expression levels of 5,311 significant DEGs were shown using a genome circle diagram, and both upregulated and downregulated genes were primarily distributed on Chr. 1 and Chr. 2 ([Figure 4C](#)). To further reveal the functions of these DEGs in GU, relevant bioinformatics analyses of the DEGs were carried out. The functions of Chr. 1 and Chr. 2 differed, with Chr. 1 focused on cellular processes and Chr. 2 on metabolic processes. A cluster analysis was performed on the DEGs based on the similarity of the gene expression profiles among the samples, and a hierarchical cluster heatmap of genes with shared differences was generated ([Figure 4D](#)). Compared with the control group, the model group had 591 upregulated and 653 downregulated DEGs. After EA intervention using different acupoint combinations, there were 1044 upregulated and 253 downregulated DEGs in the H-M group, 379 upregulated and 27 downregulated DEGs in the S-M group, and 128 upregulated and 156 downregulated DEGs in the Y-L group compared with the model group ([Figure 4E](#)).

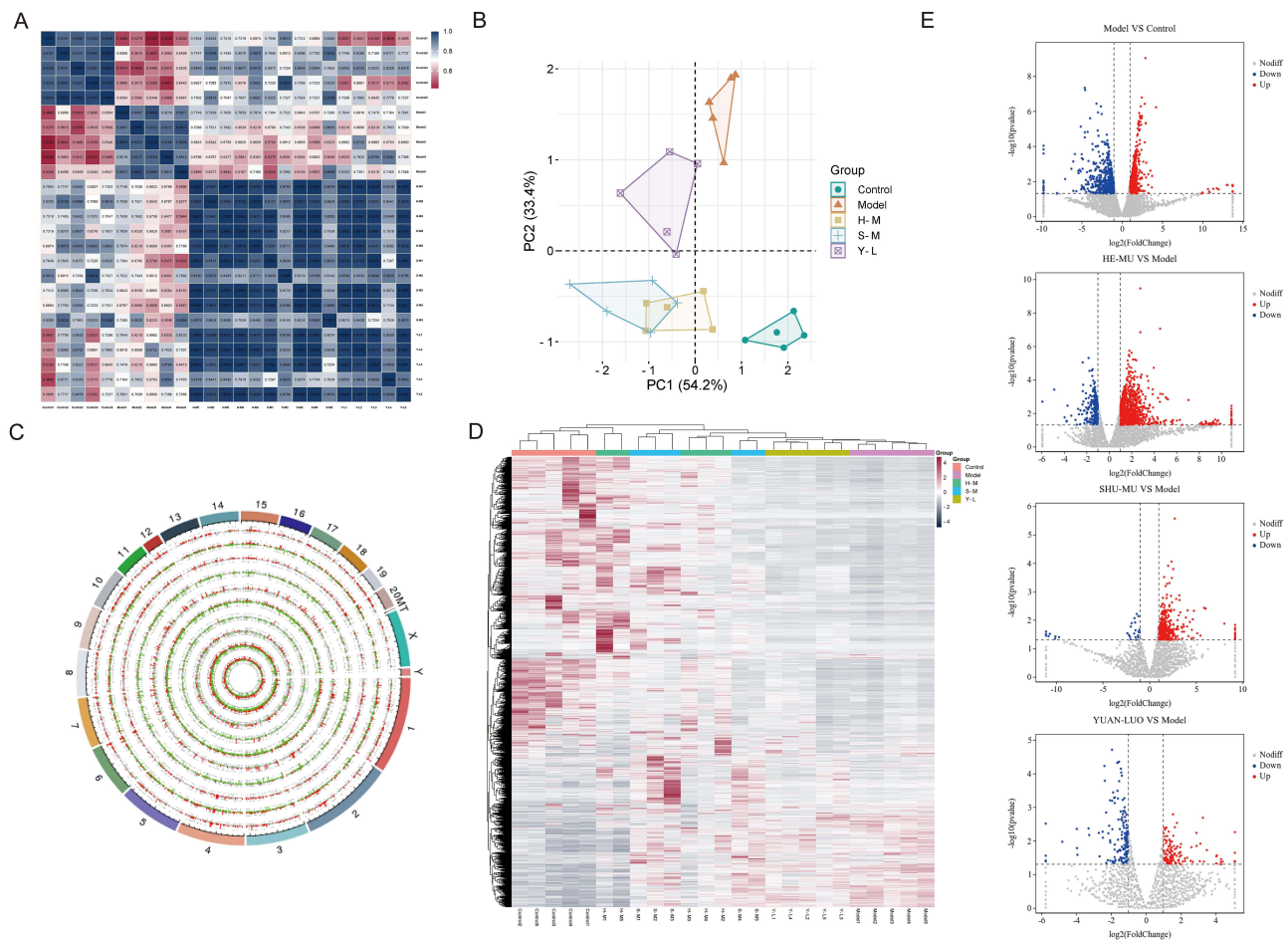


Figure 4 Results of transcriptome profiling. **(A)** Pearson correlation analysis. **(B)** PCA analysis. **(C)** Genome circle diagram. **(D)** Hierarchical cluster heatmap. **(E)** Volcano plot of DEGs.

Functional Enrichment Analysis of DEGs

To comprehensively elucidate the functions and pathways of DEGs in the pathogenesis of GU and the therapeutic effects of EA in the different acupoint combination groups, a pairwise comparison method was used for GO function and KEGG pathway enrichment analysis. The top 20 enriched pathways with the number of genes annotated in each pathway are summarized in Figure 5A. The DEGs in the model group vs control group were mainly enriched in immune-inflammatory processes (including cytokine-cytokine receptor interaction and inflammatory bowel disease), cell adhesion processes (including cell adhesion molecules and focal adhesion), and inflammatory pathways (including MAPK, NF-kappa B, IL-17, and TNF signaling pathways), which had been implicated in the pathophysiology of GU. These pathways were also partially enriched by EA in the different acupoint combination groups vs the model group, suggesting that they were strongly correlated with GU. GO functions included three categories, which were biological processes (green), cellular components (orange), and molecular functions (yellow), as shown in Figure 5B.

To delineate the molecular mechanism of the effects on GU of EA with different acupoint combinations, an overlap analysis was performed on the GO functions and KEGG pathways of the DEGs in the model group and the different acupoint combination groups (Figure 5C and D). To identify co-regulated biological pathways and molecular functions, a Venn diagram analysis was used to identify the intersection of the functional modules associated with pathways and processes regulated by DEGs, using KEGG enrichment and GO annotation datasets as reference gene sets, to systematically reveal key candidate clusters of biological pathways and functions coordinating the regulatory mechanisms of EA in GU. The results revealed that the molecular mechanisms responsible for the different effects were involved in three intersecting biological pathways: focal adhesion, Inflammatory bowel disease, and hypertrophic cardiomyopathy (Figure 5C). DEGs in these pathways were mainly

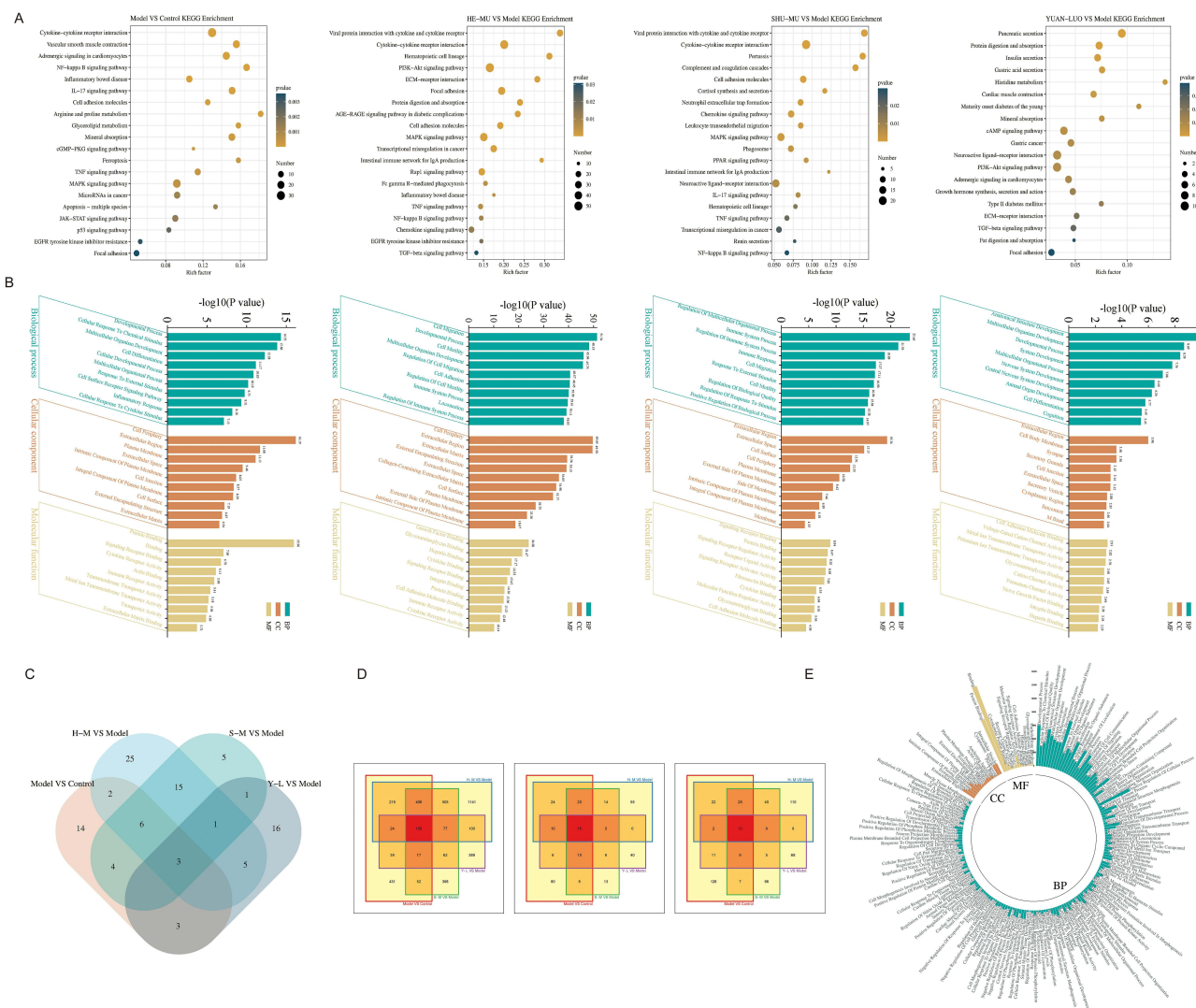


Figure 5 Functional enrichment analysis of DEGs. **(A)** KEGG pathway enrichment analysis comparing the model and control groups, as well as the H-M, S-M, Y-L, and model groups. **(B)** GO function enrichment analysis comparing the model and control groups, as well as the H-M, S-M, Y-L, and model groups. **(C)** Venn diagram analysis depicting overlapping pathways among groups. **(D)** Venn diagram analysis depicting overlapping biological processes, cellular components, and molecular functions among groups. **(E)** Polar coordinate bar diagram of overlapping GO function enrichment.

involved in 158 biological processes, 16 cellular components, and 13 molecular functions (Figure 5D), and a polar coordinate bar chart diagram of the GO function enrichment was generated (Figure 5E). GO enrichment analysis showed that the biological processes involved in the intersecting DEGs mainly included developmental processes, responses to external stimulus, inflammatory responses, and regulation of phosphorylation; the cellular components were mainly enriched in the extracellular region, extracellular space, plasma membrane, actin cytoskeleton, and other regions; and molecular functions mainly included a variety of binding functions (protein binding, cytoskeletal protein binding, cell adhesion molecule binding), and regulatory functions (receptor ligand activity, molecular function regulator activity). These results indicated that cell adhesion molecule-related pathways and gene expression had a core role and broad impact on the differential effects of GU treatment by EA in the different acupoint combination groups.

Verification of DEGs and Proteins Related to the Focal Adhesion Pathway

Using the transcriptomic data, we found that the focal adhesion pathway was the core pathway of the overlapping DEGs among the three treatment groups and the model group, which was involved in physiological and pathological processes such as the inflammatory response, phosphorylation regulation, and stimulus responses. To confirm this result, we examined the

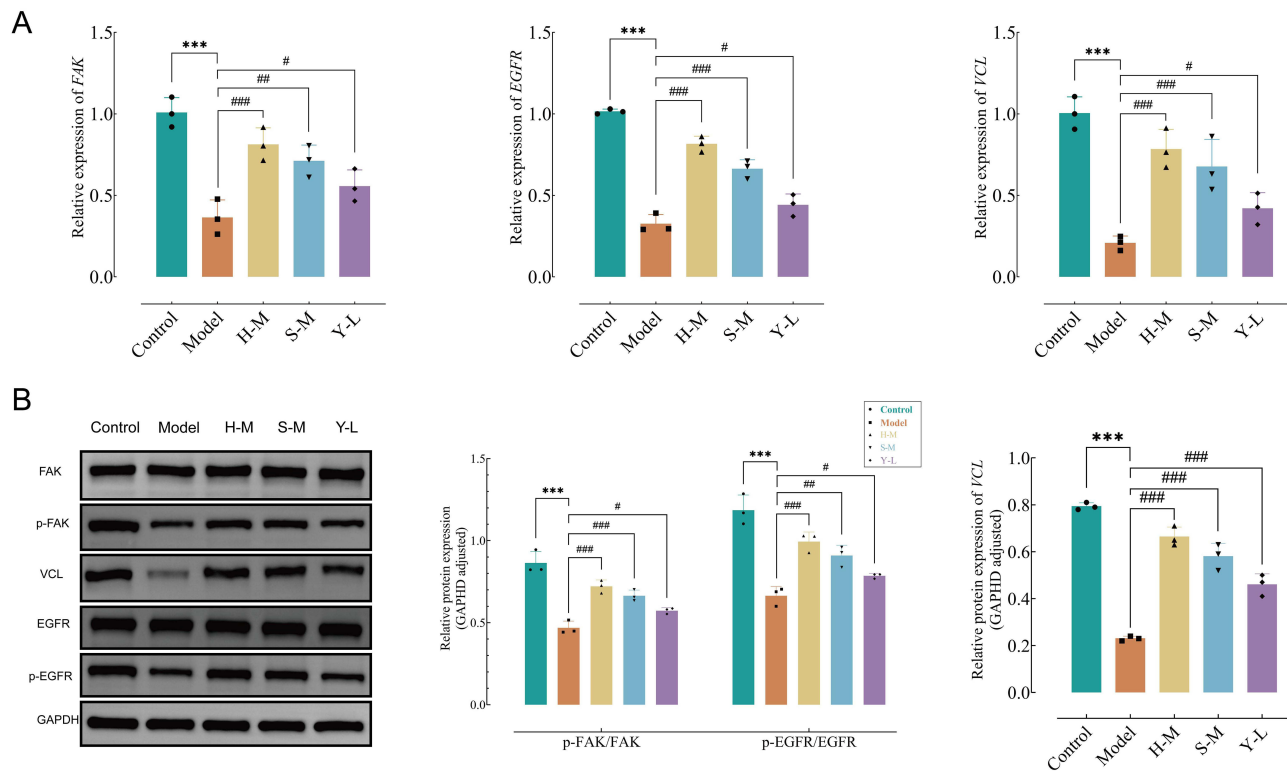


Figure 6 RT-qPCR and WB results. **(A)** RT-qPCR results for *FAK*, *VCL*, and *EGFR*. **(B)** WB results for p-*FAK*/*FAK*, p-*EGFR*/*EGFR*, *VCL*. *** $p < 0.001$ vs control group; # $p < 0.05$, ## $p < 0.01$, and ### $p < 0.001$ vs model group.

DEGs (Figure 6A) and proteins (Figure 6B) of the core signal transduction factors in the focal adhesion pathway for further validation. The gastric tissue *FAK*, *VCL*, and *EGFR* mRNA expression levels in rats from the model group were markedly decreased compared to those of the control group ($p < 0.001$), and the protein expression levels of p-*FAK*/*FAK* ($p < 0.01$), p-*EGFR*/*EGFR* ($p < 0.001$), *VCL* ($p < 0.001$) were downregulated in the model group. Compared with the model group, the same levels in the EA groups with different acupoint combinations showed varying degrees of attenuation, with the most significant differential expression observed in the H-M group. To summarize, the molecular mechanism underlying the different effects on GU by EA treatment with different acupoint combinations was involved in regulating the expression of core genes and proteins in focal adhesion. The H-M acupoint combination had the greatest upregulation of the core focal adhesion gene and protein expression levels, which increased the strength of cell adhesion, thereby increasing the resistance to mucosal damage caused by oxidative stress and inflammatory reactions.

Discussion

Gastric ulcer is a condition characterized by the destruction of gastric epithelial cells and intercellular connections due to reverse osmosis of gastric acid or pepsin, which leads to gastric mucosal injury and invasion of the muscularis mucosa.⁴³ Previous studies convincingly demonstrated the unique advantages of EA in early prevention and clinical therapy.^{44–46} However, the specificity and synergistic effect of acupoint selection required further clarification and confirmation through research on the underlying biological mechanisms. In this study, we objectively evaluated the differences in the therapeutic efficacy of the stomach meridian He-Mu, Shu-Mu, Yuan-Luo acupoint combinations on gastric mucosal injury using a GU rat model. We then selected the optimal acupoint combination group among the three, and explored the specific regulatory effects and its mechanism that provided the superior efficacy.

The GU animal model has gained international recognition for its high symptom similarity and model stability.²³ The HRWIS model specifically replicates the pathophysiological features of visceral hypersensitivity and gastrointestinal inflammation.⁴⁷ Physical restraint-induced restriction of behavioral activities induces physiological stress, while

hypothermic water immersion elicits psychological distress through the activation of tension and pressure responses in the body, which collectively contribute to immune disorder and systemic multi-organ pathological alterations.⁴⁸⁻⁵⁰ The stomach is the most sensitive organ of the human body to stress, and stress injury has been identified as an important factor driving the pathological process of GU.^{51,52} The coat appearance, fecal consistency, and visceral pain threshold of the rats serve as behavioral indicators to evaluate the severity of pathophysiological alterations in experimental models. This study demonstrated that EA intervention using different acupoint combinations ameliorated stress-induced pathophenotypes according to macroscopic indicators to varying degrees.

The gastric mucosal barrier is the first protection against gastric mucosal injury, and gastric histomorphology is a visual indicator for evaluating the integrity of the gastric mucosal barrier.⁵³ The UI and UIR are direct parameters reflecting gastric mucosal damage and repair.⁵⁴ Patients with GU often experience insufficient food intake owing to gastrointestinal discomfort, which results in weight loss and immune dysfunction in the short term.⁵⁵ The volume and quality of immune organs are important nonspecific indicators of the body's immune system status.⁵⁶ The liver, spleen, and thymus play important roles in the systemic innate immune response.⁵⁷ These organs have a unique immune microenvironment that controls the release of cytokines from the peripheral immune system, serving as a second line of defense against gastrointestinal barrier disruption and the escape of inflammatory factors.⁵⁸ The results of GU modeling showed that the body weight of the rats was significantly reduced, with pathological damage causing local gastric tissue congestion and edema, increasing the UI, gastric organ indices, and immune organ indices of the rats, thus confirming the consistency of the GU model with clinical manifestations. The pathological evaluations using HE and AB-PAS staining further verified the degree of damage to the mucosal and mucous layers of the gastric mucosal tissue. Levels of the inflammatory cytokines IL-10, IL-6, IL-4, and INF- γ , along with oxidative stress markers SOD, NO, and MDA, also increased. These findings collectively indicated oxidative stress damage and severe inflammatory responses in gastric tissue, confirming the efficacy of the GU model for clinical research at the molecular level. The application of EA at the He-Mu, Shu-Mu, and Yuan-Luo acupoint combinations regulated oxidative stress to normal levels, reduced inflammatory cell infiltration into gastric tissue, which subsequently improved gastric mucosal injury. The dynamic alterations in these biomarker levels reflected graded tissue restoration within the gastric mucosa, with a therapeutic effect in the following order: He-Mu > Shu-Mu > Yuan-Luo.

Next, to explore the possible molecular mechanisms underlying the differences in the therapeutic efficacy at the gene level, we performed transcriptome sequencing and obtained 23,096 DEGs. To reveal the pathways and biological processes associated with the differences among the acupoint combinations, we conducted GO functional and KEGG pathway enrichment analyses on the DEGs in each group. We found that EA using different acupoint combination groups to treat GU mainly included the following related functions and pathways: immune-inflammatory processes, cell adhesion processes, and inflammatory pathways. A correlation analysis was conducted on the differential pathways common to the three acupoint combination groups based on a Venn diagram. After excluding disease-associated signaling pathways, the focal adhesion pathway emerged as the enriched mechanistic pathway. Additionally, the intersection of the GO function annotation analysis of the EA acupoint combination groups identified relevant molecular functions (such as cell adhesion molecule binding and cytoskeletal protein binding located in the actin cytoskeleton) and biological processes (such as inflammatory responses and regulation of phosphorylation). Accordingly, we inferred that focal adhesion was the core pathway that produced differences in the therapeutic efficacy of EA treatment of GU with different acupoint combination groups, and that EA could have regulated the structure and function of the gastric mucosal barrier by affecting the adhesion strength and shape of gastric mucosal epithelial cells. It has been reported that applying electrical stimulation to these cells causes enlargement of focal adhesions and thickening of stress fibers.^{59,60} By regulating cell proliferation and differentiation, tyrosine phosphorylation of focal adhesions and stress fibers in the cells changed the morphology of cytoskeleton components.⁶¹ It was shown that activated and phosphorylated EGFR/Src/FAK pathways regulated the expression of tight junction proteins, which accelerated the recovery of epithelial cells.⁶² One study also showed that genes and metabolites related to the focal adhesion pathway were potential diagnostic and therapeutic targets for gastric cancer.⁶³ However, there are few reports on the involvement of the focal adhesion pathway in the EA treatment of GU at specific acupoints. Our results provide evidence for the first time that EA applied using different acupoint combinations ameliorates gastric mucosal injury by regulating the focal adhesion pathways.

Subsequently, we selected the DEGs *FAK*, *VCL*, and *EGFR*, which were core signal transduction factors in the focal adhesion pathway, for verification. Focal adhesion kinase (FAK) is a key locus of genes in the focal adhesion pathway, and its autophosphorylation promotes signal transduction and adhesion-dependent cell survival.⁶⁴ FAK has been reported to promote epithelial restitution by regulating focal adhesion assembly, disassembly, and cell migration.⁶⁵ Additionally, FAK activation in vivo and in vitro promotes the healing of gastric mucosal injury and has certain anti-inflammatory properties.⁶⁶ Vinculin (VCL) is an adaptor protein that participates in the formation of focal adhesion regulating cell adhesion.⁶⁷ The inactivation of VCL is a key step in the mechanism by which gastric epithelial injury is induced, and is an essential step in the development of GU.⁶⁸ Epidermal growth factor receptor (EGFR) is a transmembrane receptor tyrosine kinase widespread in barrier tissues that directly affects intercellular junction homeostasis.⁶⁹ Our results showed that EA with different acupoint combinations was able to reverse the expression of FAK, VCL, EGFR genes, proteins, and phosphorylated proteins after GU modeling, and it enhanced the structure and function of adherens junctions, thus providing a stable microenvironment for the reconstruction and repair of the gastric mucosal barrier. Among the three acupoint combinations, He-Mu exerted the greatest attenuating effect, which was consistent with the behavior, histopathology, and molecular biology results in this study. It was confirmed that the mechanism of different acupoint combinations of EA enhanced the core signal transduction factors of focal adhesions to potentially reduce the systemic oxidative stress response and reduce inflammatory injury of the gastric mucosa.

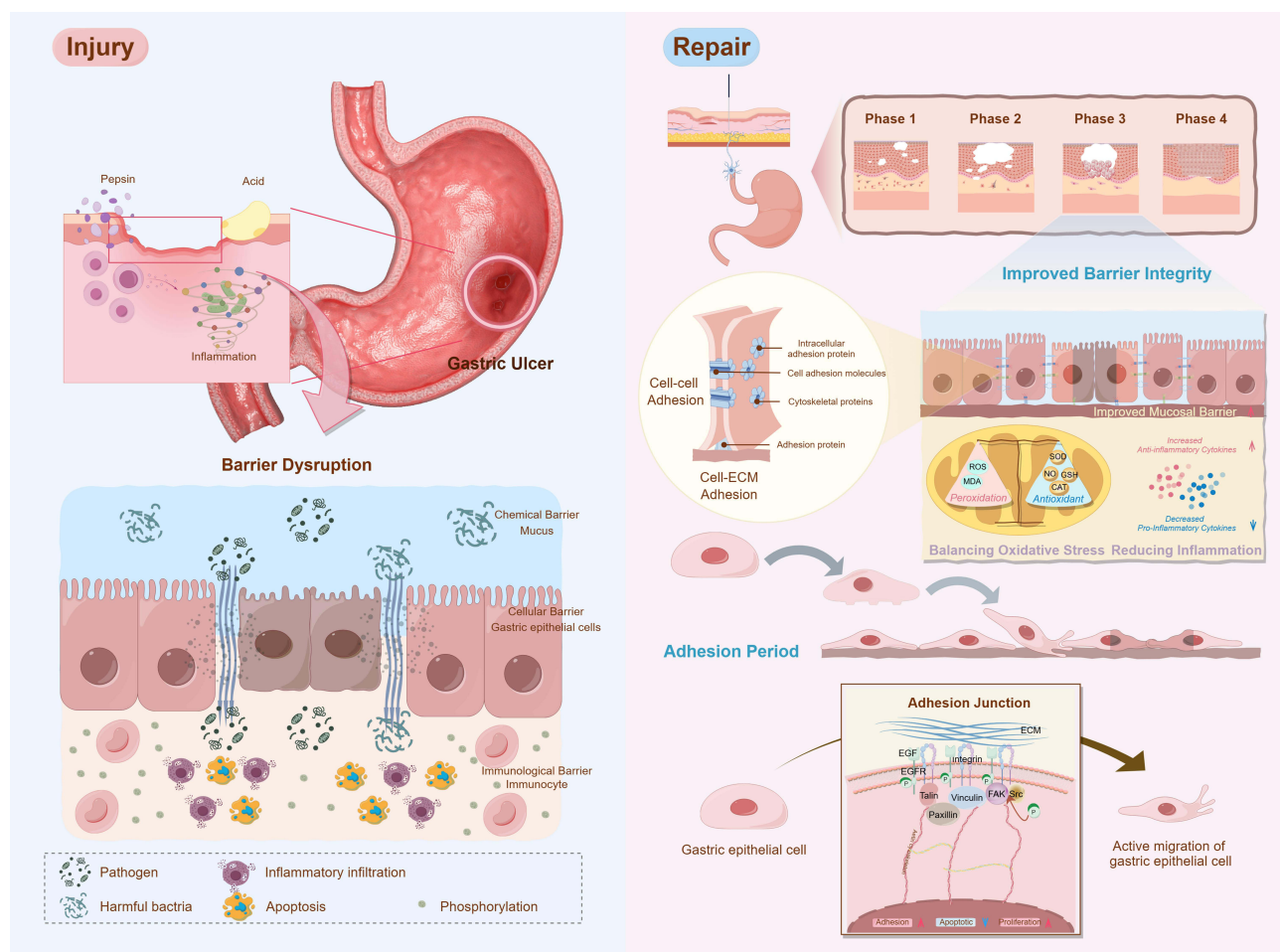


Figure 7 Mechanism of GU injury and repair by EA. Injury: Gastric ulcer pathogenesis involves acid and pepsin hypersecretion, disrupting the mucosal integrity and triggering inflammatory and apoptotic cascades that propagate tissue damage. Repair: The repair involves four phases: localized flaws, extensive atrophy and dissociation of gastric epithelial cells, cell adhesion and tissue colonization, and cell aggregation with tissue remodeling, with pivotal adhesive junction reconstruction. EA enhances cell-matrix adhesion via EGFR/FAK-Src signaling, promoting focal adhesion protein (integrin/paxillin/talin) assembly to reorganize cytoskeletal networks and the extracellular matrix, ultimately restoring mucosal barrier integrity.

In light of these results, we summarized the pathogenesis of gastric mucosal injury caused by GU and the involvement of focal adhesions EA-mediated repair (Figure 7).^{70–80} We demonstrated that EA with different acupoint combinations effectively promoted the proliferation, adhesion, and migration of gastric epithelial cells and reshaped the defense barrier structure, which significantly ameliorated oxidative stress and inflammatory damage, restored the gastric mucosal barrier, and maintained gastrointestinal homeostasis. The key to its different effects were closely related to the activation state of the focal adhesion pathway.

In summary, this study provides new insights into the molecular and physiological mechanisms underlying the specificity and synergistic effects of acupoint selection and identifies a candidate target for genetically based repair of gastric mucosal injury. Nevertheless, we acknowledge several limitations of our study. First, the study focused solely on the correlation between signaling pathways that exhibited significant expression of the DEGs also found in GU, without analyzing the potential factors or mechanisms underlying the expression of these DEGs. Future studies should explore these additional molecular mechanisms to gain a more comprehensive understanding of GU treated with EA using different acupoint combinations. Second, this study concentrated on comparing the efficacy and mechanisms of established acupoint combinations in treating GU rats; however, future studies should explore sham EA efficacy to disentangle placebo contributions, and further investigate a broader range of stimulation parameters and types to explore the appropriate dose-effect relationship between acupoint specificity and EA. Third, differences between animal experiments and clinical trials remain, and corroboration between *in vivo* and *in vitro* animal studies and clinical trials has yet to be achieved. Therefore, additional experimental studies are needed in the future to clarify the interrelationships between the mechanistic pathways, and to validate these mechanisms in clinical human subjects.

Conclusion

Our present study demonstrated that all three acupoint combinations of EA improved gastric mucosal injury in GU model rats. The He-Mu acupoint combination had the greatest effect in reducing the GU-induced inflammatory response and oxidative stress damage in gastric tissues. Transcriptome sequencing revealed that the focal adhesion pathway played an important role in EA's regulation of different acupoint combinations. In addition, we validated the differential expression of genes and proteins related to the focal adhesion pathway based on the transcriptional analysis results, and found that the He-Mu acupoint combination could positively regulate the adhesion ability of normal gastric mucosal epithelial cells on the gastric mucosa. This was associated with increased expression of the core signal transduction factors FAK, VCL, and EGFR, generating a high-adhesion phenotype and promoting gastric mucosal repair. Our study provided evidence and novel perspectives on the potential mechanism underlying the differential effects of EA in repairing GU tissue through different acupoint combinations, supported by initial *in vitro* experiments. However, the precise underlying mechanisms need additional validation and refinement through broader and more comprehensive research in the future.

Abbreviations

GU, gastric ulcer; EA, electroacupuncture; H-M, He-Mu acupoint combination; S-M, Shu-Mu acupoint combination; Y-L, Yuan-Luo acupoint combination; UI, ulcer index; UIR, ulcer inhibition ratio; HE, hematoxylin-eosin; AB-PAS, alcian blue-periodate Schiff; IL-10, interleukin 10; IL-6, interleukin 6; IL-4, interleukin 4; INF- γ , interferon γ ; SOD, superoxide dismutase; NO, nitric oxide; MDA, malondialdehyde; GO, Gene Ontology; KEGG, Kyoto Encyclopedia of Genes and Genomes; FAK, focal adhesion kinase; VCL, vinculin; EGFR, epidermal growth factor receptor; EGF, epidermal growth factor; ECM, extracellular matrix; INT, integrin; PXN, paxillin; TLN, talin; Src, steroid receptor coactivator; ROS, reactive oxygen species; CAT, catalase; GSH, glutathione; ELISA, enzyme-linked immunosorbent assay; RT-qPCR, real-time quantitative polymerase chain reaction; PCR, polymerase chain reaction; WB, Western blot.

Data Sharing Statement

The original contributions presented in the study are included in the article. Further inquiries can be directed to the corresponding author.

Ethics Approval and Informed Consent

All procedures involving animals were approved by the Animal Ethics Committee of Changchun University of Chinese Medicine (2022-08) (Jilin, China).

Acknowledgments

We sincerely appreciate the efforts of all authors who contributed to this study.

Author Contributions

All authors contributed significantly to the work, including conception, study design, execution, data acquisition, analysis and interpretation, or in all these areas. They all participated in drafting, revising, or critically reviewing the article, approved the final version for publication, agreed on the journal submission, and accept accountability for all aspects of the work.

Funding

This study was supported by the National Natural Science Foundation of China (Grant Nos. 82374600, 82004472) and the Seventh Batch of Jilin Province Youth Science and Technology Talent Support Project (Grant No. QT202319).

Disclosure

All authors disclose no competing interests in this work.

References

- Kamada T, Satoh K, Itoh T, et al. Evidence-based clinical practice guidelines for peptic ulcer disease 2020. *J Gastroenterol.* 2021;56(4):303–322. doi:10.1007/s00535-021-01769-0
- Zhang WW, Wang XF, Yu HY, Wang LF. Influence of a diet meal plan on pepsinogen I and II, gastrin-17, and nutritional status in gastric ulcer patients. *World J Clin Cases.* 2024;12(21):4574–4581. doi:10.12998/wjcc.v12.i21.4574
- Alfadil A. Gastroprotective effect of 2,3-dimethylquinoxaline against indomethacin-induced gastric ulcer in rat. *J Inflamm Res.* 2024;17:1983–1994. doi:10.2147/JIR.S453425
- Kazmi I, Saleem S, Ahmad T, et al. Protective effect of oleane-12-en-3 β -ol-28-oic acid 3 β -D-glucopyranoside in ethanol induced gastric ulcer by enhancing the prostaglandin E2 level. *J Ethnopharmacol.* 2018;211:394–399. doi:10.1016/j.jep.2017.09.012
- Tamaddonfard E, Erfanparast A, Farshid AA, et al. Safranal, a constituent of saffron, exerts gastro-protective effects against indomethacin-induced gastric ulcer. *Life Sci.* 2019;224:88–94. doi:10.1016/j.lfs.2019.03.054
- Taheri Mirghaed M, Ghasemian SO, Mousavi Nasab SF, Rahimi K. Effects of fish oil on ethanol-induced gastric ulcer in rats: inflammatory responses and oxidative stress. *Ann Med Surg.* 2024;86(2):819–825. doi:10.1097/MS9.0000000000001550
- Gupta A, Shetty S, Mutalik S, et al. Treatment of H. pylori infection and gastric ulcer: need for novel pharmaceutical formulation. *Heliyon.* 2023;9(10):e20406. doi:10.1016/j.heliyon.2023.e20406
- Gong H, Zhao N, Zhu C, Luo L, Liu S. Treatment of gastric ulcer, traditional Chinese medicine may be a better choice. *J Ethnopharmacol.* 2024;324:117793. doi:10.1016/j.jep.2024.117793
- Öztekin C, Öztekin A. Global trends in acupuncture research: a scientometric analysis from 1980 to 2023. *Medicine.* 2024;103(36):e39549. doi:10.1097/MD.00000000000039549
- Sun LQ, Luo FL, Chen S, et al. Acupuncture as an adjunctive therapy for gastric ulcer: a modified Delphi consensus study. *Complement Ther Med.* 2023;79:102997. doi:10.1016/j.ctim.2023.102997
- Wang H, Jiang H, Zhao J, et al. Acupuncture therapy for gastric ulcer: a protocol for systematic review and meta-analysis. *Medicine.* 2021;100(43):e27656. doi:10.1097/MD.00000000000027656
- Chen M, Zhao S, Guo Y, et al. The influence of acupuncture parameters on efficacy and the possible use of acupuncture in combination with or as a substitute for drug therapy in patients with ulcerative colitis. *Evid Based Complement Alternat Med.* 2022;2022:8362892. doi:10.1155/2022/8362892
- Hou Y, Lu J, Xie J, et al. Effects of electroacupuncture on perioperative anxiety and stress response in patients undergoing surgery for gastric or colorectal cancer: study protocol for a randomized controlled trial. *Front Psychiatry.* 2023;14:1095650. doi:10.3389/fpsy.2023.1095650
- Chen Y, Cai M, Shen B, Fan C, Zhou X. Electroacupuncture at Zusanli regulates the pathological phenotype of inflammatory bowel disease by modulating the NLRP3 inflammasome pathway. *Immun Inflamm Dis.* 2024;12(8):e1366. doi:10.1002/iid3.1366
- Zhang RY, Zhu BF, Zhao JG, Zhao L, Wang LK. Electroacupuncture stimulation alleviates inflammatory pain in male rats by suppressing oxidative stress. *Physiol Res.* 2023;72(5):657–667. doi:10.33549/physiolres.934965
- Chen KB, Wu ZW, Wang J, et al. Efficacy and safety of long-term transcutaneous electroacupuncture versus sham transcutaneous electroacupuncture for delayed gastric emptying after distal gastrectomy: study protocol for a randomized, patient-assessor blinded, controlled trial. *Trials.* 2022;23(1):189. doi:10.1186/s13063-022-06108-z
- Xiao Y, Zhou JY, Yin HZ, et al. Effect of electroacupuncture at “Neiguan” (PC 6) and “Zusanli” (ST 36) on gastrointestinal hormone in the antral tissue of rats with functional dyspepsia. *Zhongguo Zhen Jiu.* 2023;43(12):1435–1440. doi:10.13703/j.0255-2930.20230809-0007

18. Day J. Treatment of Plantar Fasciitis with the Yuan-Luo Point Pair: a Clinical Case Report. *J Acupunct Meridian Stud.* 2019;12(6):192–196. doi:10.1016/j.jams.2019.05.003
19. Yin S, Chen Y, Lei D, et al. Cerebral mechanism of puncturing at He-Mu point combination for functional dyspepsia: study protocol for a randomized controlled parallel trial. *Neural Regen Res.* 2017;12(5):831–840. doi:10.4103/1673-5374.206655
20. Guo X, Chen J, Lu Y, et al. Electroacupuncture at He-Mu points reduces P2X4 receptor expression in visceral hypersensitivity. *Neural Regen Res.* 2013;8(22):2069–2077. doi:10.3969/j.issn.1673-5374.2013.22.006
21. Li Q, Lu Y, Zhang X, et al. Brain-imaging mechanisms on female abdominal obesity treated by “Shu-Mu” Acupoint Catgut embedding and compatibility relation: study protocol for a 12-week randomized controlled trial. *Diabetes Metab Syndr Obes.* 2023;16:733–747. doi:10.2147/DMSO.S400197
22. You Y, Fu Y, Li L, et al. Systematic comparison of sequencing-based spatial transcriptomic methods. *Nat Methods.* 2024;21(9):1743–1754. doi:10.1038/s41592-024-02325-3
23. Zhao DQ, Xue H, Sun HJ. Nervous mechanisms of restraint water-immersion stress-induced gastric mucosal lesion. *World J Gastroenterol.* 2020;26(20):2533–2549. doi:10.3748/wjg.v26.i20.2533
24. Popović M, Popović N, Bokonjić D, Dobrić S. Cold restraint-induced gastric lesions in individual- and group-stressed rats. *Int J Neurosci.* 1997;91(1–2):1–10. doi:10.3109/00207459708986361
25. Li M, Jin X, Zhou X, et al. Effectiveness and safety of a newly designed self-assembling gel in the treatment of endoscopic submucosal dissection-induced gastric ulcer: a multicenter randomized controlled trial. *Front Pharmacol.* 2022;13:1002381. doi:10.3389/fphar.2022.1002381
26. Idris S, Mishra A, Khushfar M. Phytochemical estimation and therapeutic amelioration of *Aesculus hippocastanum* L. Seeds ethanolic extract in gastric ulcer in rats possibly by inhibiting prostaglandin synthesis. *Chin J Integr Med.* 2023;29(9):818–824. doi:10.1007/s11655-023-3734-9
27. Han SP, Han JS. Acupuncture and related techniques for pain relief and treatment of Heroin Addiction: mechanisms and clinical application. *Med Acupunct.* 2020;32(6):403–404. doi:10.1089/acu.2020.1485
28. Leung AY, Kim SJ, Schulteis G, Yaksh T. The effect of acupuncture duration on analgesia and peripheral sensory thresholds. *BMC Complement Altern Med.* 2008;8:18. doi:10.1186/1472-6882-8-18
29. Cao F, Li T, Ha LJ, Shan CX, Zhi MJ, Wang FC. Analysis of compatibility laws for acupoint selection of acupuncture in treating diabetic gastroparesis. *Zhongguo Zhong Xi Yi Jie He Za Zhi.* 2016;36(5):549–552.
30. Ji J, Huang Y, Wang XF, et al. Review of clinical studies of the treatment of ulcerative colitis using acupuncture and moxibustion. *Gastroenterol Res Pract.* 2016;2016:9248589. doi:10.1155/2016/9248589
31. Zeng F, Song WZ, Liu XG, et al. Brain areas involved in acupuncture treatment on functional dyspepsia patients: a PET-CT study. *Neurosci Lett.* 2009;456(1):6–10. doi:10.1016/j.neulet.2009.03.080
32. Li L, Qi W, Wang ZH, et al. Acupuncture preconditioning at “Zusanli” (ST36) and “Zhongwan” (CV12) prevents stress gastric ulcer by regulating the TLR4/MyD88/IκB signaling pathway. *Zhen Ci Yan Jiu.* 2021;46(3):173–179. doi:10.13702/j.1000-0607.200963
33. Li L, Zang H, Jiang Y, et al. Acupuncture at Back-Shu and Front-Mu acupoints prevents gastric ulcer by regulating the TLR4/MyD88/NF-κB signaling pathway. *Evid Based Complement Alternat Med.* 2021;2021:8214052. doi:10.1155/2021/8214052
34. Hunold A, Hauelsen J, Freitag CM, Simiatchkin M, Moliadze V. Cortical current density magnitudes during transcranial direct current stimulation correlate with skull thickness in children, adolescent and young adults. *Prog Brain Res.* 2021;264:41–56. doi:10.1016/bs.pbr.2021.01.010
35. Choi KH, Yeon SH, Cho SJ, et al. Biological safety of electroacupuncture with STS316 needles. *BMC Complement Altern Med.* 2019;19(1):285. doi:10.1186/s12906-019-2674-6
36. Tong KC, Lo SK, Cheing GL. Alternating frequencies of transcutaneous electric nerve stimulation: does it produce greater analgesic effects on mechanical and thermal pain thresholds? *Arch Phys Med Rehabil.* 2007;88(10):1344–1349. doi:10.1016/j.apmr.2007.07.017
37. Feng L, Bao T, Bai L, et al. Mongolian medicine formulae Ruda-6 alleviates indomethacin-induced gastric ulcer by regulating gut microbiome and serum metabolomics in rats. *J Ethnopharmacol.* 2023;314:116545. doi:10.1016/j.jep.2023.116545
38. Liu L, Tang Z, Zeng Q, et al. Transcriptomic insights into different stimulation intensity of electroacupuncture in Treating COPD in rat models. *J Inflamm Res.* 2024;17:2873–2887. doi:10.2147/JIR.S458580
39. Tong X, Li B, Li J, et al. Polyethylene microplastics cooperate with *Helicobacter pylori* to promote gastric injury and inflammation in mice. *Chemosphere.* 2022;288(Pt 2):132579. doi:10.1016/j.chemosphere.2021.132579
40. Elbaz EM, Abdel Rahman AAS, El-Gazar AA, Ali BM. Protective effect of dimethyl fumarate against ethanol-provoked gastric ulcers in rats via regulation of HMGB1/TLR4/NF-κB, and PPARγ/SIRT1/Nrf2 pathways: involvement of miR-34a-5p. *Arch Biochem Biophys.* 2024;759:110103. doi:10.1016/j.abb.2024.110103
41. Qu Z, Jiang D, Liu Y, Hou M. Liuwei Anxiao San protects gastric mucosa from gastric ulcer in rats by regulating the JAK2/STAT3 pathway. *Tissue Cell.* 2023;83:102145. doi:10.1016/j.tice.2023.102145
42. Zhao Z, Wei G, Wang L, et al. Pretreatment with Dan-Shen-Yin granules alleviates ethanol-induced gastric mucosal damage in rats by inhibiting oxidative stress and apoptosis via Akt/Nrf2 signaling pathway. *Phytomedicine.* 2024;132:155866. doi:10.1016/j.phymed.2024.155866
43. Wang XY, Yin JY, Zhao MM, Liu SY, Nie SP, Xie MY. Gastroprotective activity of polysaccharide from *Hericium erinaceus* against ethanol-induced gastric mucosal lesion and pylorus ligation-induced gastric ulcer, and its antioxidant activities. *Carbohydr Polym.* 2018;186:100–109. doi:10.1016/j.carbpol.2018.01.004
44. Li H, Li LL, Wang J, et al. Effect of electroacupuncture on the repair of stress ulcer injury in neurocritical patients: a randomized clinical trial. *Front Med.* 2022;9:1001584. doi:10.3389/fmed.2022.1001584
45. Zhu YJ, Wu XY, Wang W, et al. Acupuncture for quality of life in gastric cancer patients undergoing adjuvant chemotherapy. *J Pain Symptom Manage.* 2022;63(2):210–220. doi:10.1016/j.jpainsymman.2021.09.009
46. Li H, Wen Q, Lu L, et al. Transcutaneous electrical acupoint stimulation combined with electroacupuncture for rapid recovery of patients after laparotomy for gastrointestinal surgery: a study protocol for a randomised controlled trial. *BMJ Open.* 2021;11(11):e053309. doi:10.1136/bmjopen-2021-053309
47. Xu D, Gao J, Gilliland M, et al. Rifaximin alters intestinal bacteria and prevents stress-induced gut inflammation and visceral hyperalgesia in rats. *Gastroenterology.* 2014;146(2):484–96.e4. doi:10.1053/j.gastro.2013.10.026
48. Yin YC, Li XH, Rao X, Li YJ, Du J. Involvement of microRNA/cystine/glutamate transporter in cold-stressed gastric mucosa injury. *Front Pharmacol.* 2022;13:968098. doi:10.3389/fphar.2022.968098

49. Fukudo S, Abe K, Hongo M, Utsumi A, Itoyama Y. Psychophysiological stress induces heat shock cognate protein (HSC) 70 mRNA in the cerebral cortex and stomach of rats. *Brain Res.* 1995;675(1–2):98–102. doi:10.1016/0006-8993(95)00044-q
50. Landeira-Fernandez J. Analysis of the cold-water restraint procedure in gastric ulceration and body temperature. *Physiol Behav.* 2004;82(5):827–833. doi:10.1016/j.physbeh.2004.06.016
51. Ray A, Gulati K, Henke P. Stress gastric ulcers and cytoprotective strategies: perspectives and trends. *Curr Pharm Des.* 2020;26(25):2982–2990. doi:10.2174/1381612826666200521143203
52. Kumar M, Singh N, Jaggi AS. Exploring the anti-stress effects of imatinib and tetrabenazine in cold-water immersion-induced acute stress in mice. *Naunyn Schmiedeberg's Arch Pharmacol.* 2020;393(9):1625–1634. doi:10.1007/s00210-020-01862-w
53. Arai J, Hayakawa Y, Tateno H, Fujiwara H, Kasuga M, Fujishiro M. The role of gastric mucins and mucin-related glycans in gastric cancers. *Cancer Sci.* 2024;115(9):2853–2861. doi:10.1111/cas.16282
54. Liu J, Fang J, Zhang J, et al. Protective effect of Anwulignan on gastric injury induced by indomethacin in mice. *J Pharmacol Exp Ther.* 2022;383(1):80–90. doi:10.1124/jpet.121.001055
55. Bailey JM. Gastrointestinal conditions: peptic ulcer disease. *FP Essent.* 2024;540:16–23.
56. Li Z, Liu S, Gao Z, et al. Dynamic proteomic changes in tumor and immune organs reveal systemic immune response to tumor development. *mol Cell Proteomics.* 2024;23(5):100756. doi:10.1016/j.mcpro.2024.100756
57. Zhang H, Sun Y, Fan M, et al. Prevention effect of total ginsenosides and ginseng extract from Panax ginseng on cyclophosphamide-induced immunosuppression in mice. *Phytother Res.* 2023;37(8):3583–3601. doi:10.1002/ptr.7836
58. Wang YN, Zhai XY, Wang Z, et al. Jianpi-Huatan-Huoxue-Anshen formula ameliorates gastrointestinal inflammation and microecological imbalance in chemotherapy-treated mice transplanted with H22 hepatocellular carcinoma. *World J Gastrointest Oncol.* 2024;16(10):4209–4231. doi:10.4251/wjgo.v16.i10.4209
59. Katoh K. Effects of electrical stimulation on the signal transduction-related proteins, c-Src and Focal Adhesion Kinase, in Fibroblasts. *Life.* 2022;12(4):531. doi:10.3390/life12040531
60. Xie Y, Han KH, Grainger N, et al. A role for focal adhesion kinase in facilitating the contractile responses of murine gastric fundus smooth muscles. *J Physiol.* 2018;596(11):2131–2146. doi:10.1113/JP275406
61. Kanchanawong P, Calderwood DA. Organization, dynamics and mechanoregulation of integrin-mediated cell-ECM adhesions. *Nat Rev mol Cell Biol.* 2023;24(2):142–161. doi:10.1038/s41580-022-00531-5
62. Huang C, Wang L, Wu G. Trefoil factor 1 (TFF1) reduces cerebral edema and gastric mucosal injury by regulating the EGFR/Src/FAK pathway in an intracerebral hemorrhage rat model. *Neuropeptides.* 2024;107:102460. doi:10.1016/j.npep.2024.102460
63. He H, Dong K, Chen M, et al. TOB1 inhibits the gastric cancer progression by focal adhesion pathway and ERK pathway based on transcriptional and metabolic sequencing. *BMC Cancer.* 2024;24(1):1130. doi:10.1186/s12885-024-12894-3
64. Aplin AE, Howe A, Alahari SK, Juliano RL. Signal transduction and signal modulation by cell adhesion receptors: the role of integrins, cadherins, immunoglobulin-cell adhesion molecules, and selectins. *Pharmacol Rev.* 1998;50(2):197–263.
65. Burridge K. Focal adhesions: a personal perspective on a half century of progress. *FEBS J.* 2017;284(20):3355–3361. doi:10.1111/febs.14195
66. Oncel S, Gupta R, Wang Q, Basson MD. ZINC40099027 promotes gastric mucosal repair in ongoing aspirin-associated gastric injury by activating focal adhesion kinase. *Cells.* 2021;10(4):908. doi:10.3390/cells10040908
67. Bidel S, Mustonen H, Khalighi-Sikaroudi G, et al. Effect of the ulcerogenic agents ethanol, acetylsalicylic acid and taurocholate on actin cytoskeleton and cell motility in cultured rat gastric mucosal cells. *World J Gastroenterol.* 2005;11(26):4032–4039. doi:10.3748/wjg.v11.i26.4032
68. Moese S, Selbach M, Brinkmann V, et al. The Helicobacter pylori CagA protein disrupts matrix adhesion of gastric epithelial cells by dephosphorylation of vinculin. *Cell Microbiol.* 2007;9(5):1148–1161. doi:10.1111/j.1462-5822.2006.00856.x
69. Zheng X, Liu L, Liu J, et al. Fibulin7 mediated pathological cardiac remodeling through EGFR binding and EGFR-dependent FAK/AKT Signaling Activation. *Adv Sci.* 2023;10(24):e2207631. doi:10.1002/adv.202207631
70. Shanmugapriya K, Kim H, Kang HW. EGFR-conjugated hydrogel accelerates wound healing on ulcer-induced burn wounds by targeting collagen and inflammatory cells using photoimmunomodulatory inhibition. *Mater Sci Eng C Mater Biol Appl.* 2021;118:111541. doi:10.1016/j.msec.2020.111541
71. Xie R, Yan X, Yu J, et al. pH-responsive bioadhesive with robust and stable wet adhesion for gastric ulcer healing. *Biomaterials.* 2024;309:122599. doi:10.1016/j.biomaterials.2024.122599
72. Ye HY, Shang ZZ, Zhang FY, Zha XQ, Li QM, Luo JP. Dendrobium huoshanense stem polysaccharide ameliorates alcohol-induced gastric ulcer in rats through Nrf2-mediated strengthening of gastric mucosal barrier. *Int J Biol Macromol.* 2023;236:124001. doi:10.1016/j.ijbiomac.2023.124001
73. Ni R, Luo Y, Jiang L, et al. Repairing gastric ulcer with hyaluronic acid/extracellular matrix composite through promoting M2-type polarization of macrophages. *Int J Biol Macromol.* 2023;245:125556. doi:10.1016/j.ijbiomac.2023.125556
74. Tang W, Guan M, Li Z, Pan W, Wang Z. A2BR facilitates the pathogenesis of H. pylori-associated GU by inducing oxidative stress through p38 MAPK phosphorylation. *Heliyon.* 2023;9(11):e21004. doi:10.1016/j.heliyon.2023.e21004
75. Li G, Liu X, Miao Z, Hu N, Zheng X. Preparation of corn peptides with anti-adhesive activity and its functionality to alleviate gastric injury induced by helicobacter pylori infection in vivo. *Nutrients.* 2023;15(15):3467. doi:10.3390/nu15153467
76. Wang W, Song L, Yang L, et al. Panax quinquefolius saponins combined with dual antiplatelet therapy enhanced platelet inhibition with alleviated gastric injury via regulating eicosanoids metabolism. *BMC Complement Med Ther.* 2023;23(1):289. doi:10.1186/s12906-023-04112-7
77. Chan GK, McGrath JA, Parsons M. Spatial activation of ezrin by epidermal growth factor receptor and focal adhesion kinase co-ordinates epithelial cell migration. *Open Biol.* 2021;11(8):210166. doi:10.1098/rsob.210166
78. Liang P, Wu Y, Zheng S, et al. Paxillin phase separation promotes focal adhesion assembly and integrin signaling. *J Cell Biol.* 2024;223(4):e202209027. doi:10.1083/jcb.202209027
79. Horton ER, Byron A, Askari JA, et al. Definition of a consensus integrin adhesome and its dynamics during adhesion complex assembly and disassembly. *Nat Cell Biol.* 2015;17(12):1577–1587. doi:10.1038/ncb3257
80. Katoh K. Focal Adhesion Kinase (FAK) and c-Src dependent signal transduction in cell adhesion. *Discov Med.* 2024;36(189):1998–2012. doi:10.24976/Discov.Med.202436189

Journal of Inflammation Research

Publish your work in this journal

The Journal of Inflammation Research is an international, peer-reviewed open-access journal that welcomes laboratory and clinical findings on the molecular basis, cell biology and pharmacology of inflammation including original research, reviews, symposium reports, hypothesis formation and commentaries on: acute/chronic inflammation; mediators of inflammation; cellular processes; molecular mechanisms; pharmacology and novel anti-inflammatory drugs; clinical conditions involving inflammation. The manuscript management system is completely online and includes a very quick and fair peer-review system. Visit <http://www.dovepress.com/testimonials.php> to read real quotes from published authors.

Submit your manuscript here: <https://www.dovepress.com/journal-of-inflammation-research-journal>

Dovepress
Taylor & Francis Group